



HAL
open science

Improving Small-Signal Stability of an MMC With CCSC by Control of the Internally Stored Energy

Julian Freytes, Gilbert Bergna, Suul Jon Are, Salvatore d'Arco, François Gruson, Frederic Colas, Hani Saad, Xavier Guillaud

► **To cite this version:**

Julian Freytes, Gilbert Bergna, Suul Jon Are, Salvatore d'Arco, François Gruson, et al.. Improving Small-Signal Stability of an MMC With CCSC by Control of the Internally Stored Energy. IEEE Transactions on Power Delivery, 2018, 33 (1), pp.429-439. 10.1109/TPWRD.2017.2725579 . hal-01760346

HAL Id: hal-01760346

<https://hal.science/hal-01760346v1>

Submitted on 6 Apr 2018

HAL is a multi-disciplinary open access archive for the deposit and dissemination of scientific research documents, whether they are published or not. The documents may come from teaching and research institutions in France or abroad, or from public or private research centers.

L'archive ouverte pluridisciplinaire **HAL**, est destinée au dépôt et à la diffusion de documents scientifiques de niveau recherche, publiés ou non, émanant des établissements d'enseignement et de recherche français ou étrangers, des laboratoires publics ou privés.

Improving Small-Signal Stability of an MMC with CCSC by Control of the Internally Stored Energy

Julian Freytes, *Student Member, IEEE*, Gilbert Bergna, Jon Are Suul, *Member, IEEE*, Salvatore D'Arco, François Gruson, Frédéric Colas, Hani Saad, *Member, IEEE* and Xavier Guillaud, *Member, IEEE*

Abstract—The DC-side dynamics of Modular Multilevel Converters (MMCs) can be prone to poorly damped oscillations or stability problems when the second harmonic components of the arm currents are mitigated by a Circulating Current Suppression Controller (CCSC). This paper demonstrates that the source of these oscillations is the uncontrolled interaction of the DC-side current and the internally stored energy of the MMC, as resulting from the CCSC. Stable operation and improved performance of the MMC control system can be ensured by introducing closed loop control of the energy and the DC-side current. The presented analysis relies on a detailed state-space model of the MMC which is formulated to obtain constant variables in steady state. The resulting state-space equations can be linearized to achieve a Linear Time Invariant (LTI) model, allowing for eigenvalue analysis of the small-signal dynamics of the MMC. Participation factor analysis is utilized to identify the source of the poorly damped DC-side oscillations, and indicates the suitability of introducing control of the internal capacitor voltage or the corresponding stored energy. An MMC connected to a DC power source with an equivalent capacitance, and operated with DC voltage droop in the active power flow control, is used as an example for the presented analysis. The developed small-signal models and the improvement in small-signal dynamics achieved by introducing control of the internally stored energy are verified by time-domain simulations in comparison to an EMT simulation model of an MMC with 400 sub-modules per arm.

Index Terms—HVDC Transmission, Modular Multilevel Converter, State-Space Modeling, Small-Signal Stability Analysis

I. INTRODUCTION

The Modular Multilevel Converter (MMC) is currently the most promising topology for High Voltage DC transmission systems (HVDC) [1]. Several advantages of the MMC compared to other topologies may be enumerated, such as lower losses, modularity, scalability and low harmonic content in the output AC voltage [1], [2]. Nevertheless, the internal dynamics of the MMC topology makes the modeling, control and stability studies of this converter highly challenging [3].

Without control of the internal dynamics, a three-phase MMC will experience large second harmonic currents circulating between the different phases, and potential resonances between the internal equivalent capacitance and the filter inductor [4]. Thus, a Circulating Current Suppression Controller (CCSC) is commonly applied for eliminating the double frequency circulating currents [5]. However, recent studies have demonstrated that poorly damped oscillations or even instability associated with the DC-side current can occur for MMCs with conventional CCSC-based control [6]–[9].

Due to the multiple frequency components naturally appearing in the internal circulating currents and the arm capacitor voltages of an MMC [10], traditional power-system-oriented approaches for state-space modeling, linearization and eigenvalue

analysis cannot be directly applied. Thus, in [8], the stability of an MMC was studied by application of time-periodic system theory (Poincaré multipliers), to demonstrate how the double frequency dq current control loops of the CCSC can make the system unstable. Similar conclusions were obtained in [6], [7], [11], by eigenvalue analysis within a modeling framework based on dynamic phasors and harmonic superposition, for separately representing the different frequency components of the internal MMC variables. However, recent modeling efforts have led to the development of state-space models that avoid the approximation of harmonic superposition. Indeed, the MMC model from [12] is first expressed in a form that separates the variables into groups with only one steady-state oscillation frequency, before the variables are transformed into their associated Synchronously Rotating Reference Frames (SRRFs). The resulting model can be linearized for application of traditional eigenvalue analysis, as demonstrated in [9] where only the *Classical CCSC* strategy was considered.

This paper extends the MMC model from [12] by including a simplified representation of the DC bus voltage dynamics in a Multi-Terminal DC grid (MTDC), represented by an equivalent capacitance and a power source. A DC voltage droop control, as expected for HVDC operation in MTDC grids [13], [14], is also included in the model.

Furthermore, the adapted state-space model is linearized, and the impact of the equivalent DC-side capacitance and the droop gain on the poorly damped oscillation modes that occur with the *Classical CCSC* are investigated by eigenvalue analysis. Participation factor analysis is applied to identify the source of these oscillations, which is shown to be mainly the interaction between the uncontrolled DC-side current and the voltage or the energy of the internal capacitance of the MMC. This indicates that the stability and control system performance can be improved by introducing closed loop control of the DC-side current and the total stored energy within the MMC. By introducing such *Energy-based* control, with a structure simplified from [14], the stability problems are avoided and good performance of the control system can be ensured for the full range of expected operating conditions. The obtained improvement in the small-signal stability is demonstrated by time-domain simulations as well as by eigenvalue analysis.

II. AVERAGED MMC MODELS FOR MATHEMATICAL ANALYSIS

In this section, the Arm Averaged Model (AAM) from [15], [16] is first presented to describe the basic mathematical relations of an MMC. Then, a time-invariant model that can

be linearized for small-signal eigenvalue analysis is developed according to the approach presented in [12].

A. Continuous time-periodic Arm Averaged Model

The Arm Averaged Model (AAM) of the MMC is recalled in Fig. 1. The model presents for each phase j ($j = a, b, c$), a leg consisting of an upper and a lower arm. Each arm includes an inductance L_{arm} , an equivalent resistance R_{arm} and an aggregated capacitance C_{arm} [15].

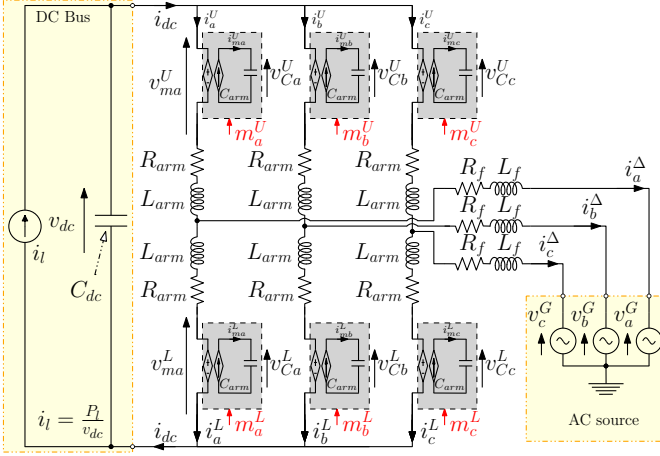


Figure 1. Schematic of the reference configuration with MMC connected to a DC bus capacitor

A simplified model is assumed for the DC bus dynamics consisting of an equivalent capacitor C_{dc} which emulates the capacitance of the DC cables and other converter stations connected to the grid. Also, in parallel with C_{dc} there is a controlled current source i_l whose output power is P_l as an equivalent model of the power exchanged in the HVDC system.

The modulated voltages v_{mj}^U and v_{mj}^L , as well as the currents i_{mj}^U and i_{mj}^L of each arm j are described as follows:

$$v_{mj}^U = m_j^U v_{Cj}^U, \quad v_{mj}^L = m_j^L v_{Cj}^L \quad (1)$$

$$i_{mj}^U = m_j^U i_j^U, \quad i_{mj}^L = m_j^L i_j^L \quad (2)$$

where m_j^U (m_j^L) is the corresponding insertion index, and v_{Cj}^U (v_{Cj}^L) is the voltage across the upper (lower) equivalent arm capacitance C_{arm} . The voltage and current of the equivalent capacitor are related by the following equation:

$$C_{arm} \frac{dv_{Cj}^U}{dt} = i_{mj}^U, \quad C_{arm} \frac{dv_{Cj}^L}{dt} = i_{mj}^L. \quad (3)$$

For deriving the current dynamics of the AAM, the modulation indexes m_j^Δ and m_j^Σ as well as modulated voltages v_{mj}^Δ and v_{mj}^Σ are introduced [16]:

$$m_j^\Delta \stackrel{\text{def}}{=} m_j^U - m_j^L, \quad m_j^\Sigma \stackrel{\text{def}}{=} m_j^U + m_j^L \quad (4)$$

$$v_{mj}^\Delta \stackrel{\text{def}}{=} (-v_{mj}^U + v_{mj}^L)/2, \quad v_{mj}^\Sigma \stackrel{\text{def}}{=} (v_{mj}^U + v_{mj}^L)/2 \quad (5)$$

The MMC currents can be expressed as:

$$i_j^\Delta \stackrel{\text{def}}{=} i_j^U - i_j^L, \quad i_j^\Sigma \stackrel{\text{def}}{=} (i_j^U + i_j^L)/2 \quad (6)$$

where i_j^Δ corresponds to the AC grid current, and i_j^Σ is the common-mode current flowing through the upper and lower arm. The current i_j^Σ is commonly referred as ‘‘circulating current’’ or ‘‘differential current’’ [16]. However, the more general term ‘‘common-mode current’’ is preferred in this paper, since i_j^Σ is calculated as a *sum* of two currents.

The AC grid current dynamics are expressed as:

$$L_{eq}^{ac} \frac{di_j^\Delta}{dt} = v_{mj}^\Delta - v_j^G - R_{eq}^{ac} i_j^\Delta \quad (7)$$

where $R_{eq}^{ac} \stackrel{\text{def}}{=} (R_{arm} + 2R_f)/2$ and $L_{eq}^{ac} \stackrel{\text{def}}{=} (L_{arm} + 2L_f)/2$. The common-mode arm currents dynamics are given by:

$$L_{arm} \frac{di_j^\Sigma}{dt} = \frac{v_{dc}}{2} - v_{mj}^\Sigma - R_{arm} i_j^\Sigma \quad (8)$$

Finally, the addition and difference of the terms in (3) yields,

$$2C_{arm} \frac{dv_{Cj}^\Sigma}{dt} = m_j^\Delta \frac{ij^\Delta}{2} + m_j^\Sigma i_j^\Sigma \quad (9)$$

$$2C_{arm} \frac{dv_{Cj}^\Delta}{dt} = m_j^\Sigma \frac{ij^\Delta}{2} + m_j^\Delta i_j^\Sigma \quad (10)$$

where $v_{Cj}^\Delta \stackrel{\text{def}}{=} (v_{Cj}^U - v_{Cj}^L)/2$ and $v_{Cj}^\Sigma \stackrel{\text{def}}{=} (v_{Cj}^U + v_{Cj}^L)/2$. With the new definitions, the modulated voltages v_{mj}^Δ and v_{mj}^Σ can be expressed as follows:

$$v_{mj}^\Delta = -\frac{1}{2} (m_j^\Delta v_{Cj}^\Sigma + m_j^\Sigma v_{Cj}^\Delta) \quad (11)$$

$$v_{mj}^\Sigma = \frac{1}{2} (m_j^\Sigma v_{Cj}^\Sigma + m_j^\Delta v_{Cj}^\Delta) \quad (12)$$

In steady state, ‘‘ Δ ’’ variables are sinusoidal at the fundamental grid frequency ω , while ‘‘ Σ ’’ variables contain a sinusoidal oscillation at -2ω superimposed to a DC-component [12]. Thus, the variables can be classified as summarized in Table I.

Table I
MMC VARIABLES IN Σ - Δ REPRESENTATION

Variables oscillating at ω	Variables oscillating at -2ω
$i_j^\Delta, v_{mj}^\Delta, m_j^\Delta, v_{Cj}^\Delta$	$i_j^\Sigma, v_{mj}^\Sigma, m_j^\Sigma, v_{Cj}^\Sigma$

In the following section, a non-linear time-invariant model is obtained from the MMC model in ‘‘ Σ - Δ ’’ representation given by (7)–(12).

B. Non-linear time-invariant model using voltage-based formulations in Σ - Δ representation

This section summarizes the time-invariant model of the MMC with voltage-based formulation as proposed in [12]. To achieve a time-invariant model, it is necessary to refer the MMC variables to their corresponding SRRFs, following the frequency classification shown in Table I. For generic variables x^Σ and x^Δ , time-invariant equivalents are obtained with the Park transformation defined in (13) as (bold variables means matrix or vectors):

$$\omega \Rightarrow \mathbf{x}_{dqz}^\Delta \stackrel{\text{def}}{=} \begin{bmatrix} x_d^\Delta & x_q^\Delta & x_z^\Delta \end{bmatrix}^\top = \mathbf{P}_\omega \begin{bmatrix} x_a^\Delta & x_b^\Delta & x_c^\Delta \end{bmatrix}^\top$$

$$-2\omega \Rightarrow \mathbf{x}_{dqz}^\Sigma \stackrel{\text{def}}{=} \begin{bmatrix} x_d^\Sigma & x_q^\Sigma & x_z^\Sigma \end{bmatrix}^\top = \mathbf{P}_{-2\omega} \begin{bmatrix} x_a^\Sigma & x_b^\Sigma & x_c^\Sigma \end{bmatrix}^\top$$

$$\mathbf{P}_{n\omega} = \frac{2}{3} \begin{bmatrix} \cos(n\omega t) & \cos(n\omega t - \frac{2\pi}{3}) & \cos(n\omega t - \frac{4\pi}{3}) \\ \sin(n\omega t) & \sin(n\omega t - \frac{2\pi}{3}) & \sin(n\omega t - \frac{4\pi}{3}) \\ \frac{1}{2} & \frac{1}{2} & \frac{1}{2} \end{bmatrix} \quad (13)$$

The formulation of the MMC variables such that this initial separation of frequency components can be achieved constitutes the basis for the used modelling approach, as illustrated in Fig. 2.

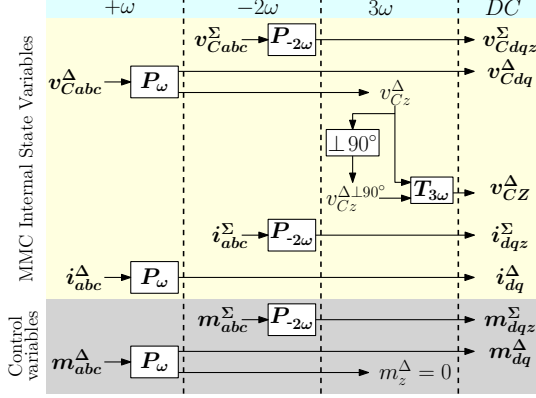


Figure 2. The used modelling approach based on three Park transformations to achieve SSTI state variables

As shown in (7)–(12), the Σ and Δ quantities are not fully decoupled. This results in time-periodic variables in the equations after applying the above transformations. For the Σ variables, time-periodic terms of 6ω are neglected without compromising the accuracy of the model. Conversely, the zero sequences of the vectors in “ Δ ” variables present time-periodic terms of 3ω which has to be taken into account. This component was modeled by means of an auxiliary virtual variable, 90° shifted from the real one, and by using a transformation $\mathbf{T}_{3\omega}$ at $+3\omega$ to achieve a model with a defined equilibrium point.

$$3\omega^+ \Rightarrow \mathbf{x}_Z^\Delta \stackrel{\text{def}}{=} \begin{bmatrix} x_{Zd}^\Delta \\ x_{Zq}^\Delta \end{bmatrix} = \underbrace{\begin{bmatrix} \cos(3\omega) & \sin(3\omega) \\ \sin(3\omega) & -\cos(3\omega) \end{bmatrix}}_{\mathbf{T}_{3\omega}} \begin{bmatrix} x_z^\Delta \\ x_z^{90^\circ} \end{bmatrix}$$

Using the above definitions, the MMC dynamics in their “ Σ - Δ ” representation can be reformulated as a state-space model where all states reach constant values in steady-state [12]. The resulting system is recalled in the following.

1) *AC grid currents*: Applying the Park transformation at ω to (7), the SRRF representation of the AC side current dynamics i_{dq}^Δ are given as:

$$L_{eq}^{ac} \frac{di_{dq}^\Delta}{dt} = -\mathbf{v}_{dq}^G + \mathbf{v}_{mdq}^\Delta - R_{eq}^{ac} i_{dq}^\Delta - \mathbf{J}_\omega L_{eq}^{ac} i_{dq}^\Delta \quad (14)$$

where \mathbf{v}_{dq}^G is the grid voltage at the point of interconnection and \mathbf{J}_ω is the cross-coupling matrix at the fundamental frequency, as defined in (15),

$$\mathbf{J}_\omega \stackrel{\text{def}}{=} \begin{bmatrix} 0 & \omega \\ -\omega & 0 \end{bmatrix}. \quad (15)$$

The AC-side modulated voltage \mathbf{v}_{mdq}^Δ is defined in (16) as a function of the modulation indexes \mathbf{m}_{dq}^Δ and \mathbf{m}_{dqz}^Σ ,

$$\mathbf{v}_{mdq}^\Delta = \frac{1}{4} \mathbf{V}^\Delta \left[\mathbf{m}_{dq}^\Delta{}^\top, \mathbf{m}_{dq}^\Sigma{}^\top, m_z^\Sigma \right]^\top. \quad (16)$$

\mathbf{V}^Δ is defined as the following 2×5 voltage matrix, where all elements are represented in their associated SRRFs:

$$\mathbf{V}^\Delta \stackrel{\text{def}}{=} \begin{bmatrix} -2v_{Cz}^\Sigma - v_{Cd}^\Sigma & v_{Cq}^\Sigma & -v_{Cd}^\Delta - v_{CZd}^\Delta & v_{Cq}^\Delta + v_{CZq}^\Delta & -2v_{Cd}^\Delta \\ v_{Cz}^\Sigma & v_{Cz}^\Sigma - 2v_{Cz}^\Sigma & v_{Cq}^\Delta - v_{CZq}^\Delta & v_{Cd}^\Delta - v_{CZd}^\Delta & -2v_{Cq}^\Delta \end{bmatrix}. \quad (17)$$

2) *Common-mode arm currents*: Similarly, applying the Park transformation at -2ω to (8), the dynamics of the common-mode arm currents in their time invariant representation i_{dq}^Σ and i_z^Σ are obtained, shown in (18a).

$$L_{arm} \frac{di_{dq}^\Sigma}{dt} = -\mathbf{v}_{mdq}^\Sigma - R_{arm} i_{dq}^\Sigma - 2\mathbf{J}_\omega L_{arm} i_{dq}^\Sigma \quad (18a)$$

$$L_{arm} \frac{di_z^\Sigma}{dt} = -v_{mz}^\Sigma - R_{arm} i_z^\Sigma + \frac{v_{dc}}{2} \quad (18b)$$

with v_{dc} representing the voltage at the MMC DC terminals. The modulated voltages driving the currents i_{dq}^Σ and i_z^Σ are \mathbf{v}_{mdq}^Σ and v_{mz}^Σ . These voltages are defined in (19), as a function of the modulation indexes:

$$\mathbf{v}_{mdqz}^\Sigma = \frac{1}{4} \mathbf{V}^\Sigma \left[\mathbf{m}_{dq}^\Delta{}^\top, \mathbf{m}_{dq}^\Sigma{}^\top, m_z^\Sigma \right]^\top. \quad (19)$$

\mathbf{V}^Σ corresponds to the following 3×5 voltage matrix:

$$\mathbf{V}^\Sigma \stackrel{\text{def}}{=} \begin{bmatrix} v_{Cd}^\Delta + v_{CZd}^\Delta & -v_{Cq}^\Delta + v_{CZq}^\Delta & 2v_{Cz}^\Sigma & 0 & 2v_{Cd}^\Sigma \\ -v_{Cq}^\Delta - v_{CZq}^\Delta & -v_{Cd}^\Delta + v_{CZd}^\Delta & 0 & 2v_{Cz}^\Sigma & 2v_{Cq}^\Sigma \\ v_{Cd}^\Delta & v_{Cq}^\Delta & v_{Cd}^\Sigma & v_{Cq}^\Sigma & 2v_{Cz}^\Sigma \end{bmatrix}. \quad (20)$$

3) *Arm capacitor voltages sum*: Applying the Park transformation at -2ω to (9), the time invariant dynamics of the voltage sum vector \mathbf{v}_{Cdqz}^Σ can be expressed by (21).

$$C_{arm} \frac{d\mathbf{v}_{Cdqz}^\Sigma}{dt} = i_{mdqz}^\Sigma - \begin{bmatrix} -2\mathbf{J}_\omega & \mathbf{0}_{2 \times 1} \\ \mathbf{0}_{1 \times 2} & 0 \end{bmatrix} C_{arm} \mathbf{v}_{Cdqz}^\Sigma \quad (21)$$

with i_{mdqz}^Σ representing the modulated current as defined in (22), as a function of the modulation indexes,

$$i_{mdqz}^\Sigma = \frac{1}{8} \mathbf{I}^\Sigma \left[\mathbf{m}_{dq}^\Delta{}^\top, \mathbf{m}_{dq}^\Sigma{}^\top, m_z^\Sigma \right]^\top. \quad (22)$$

\mathbf{I}^Σ is the following 3×5 time invariant current matrix:

$$\mathbf{I}^\Sigma \stackrel{\text{def}}{=} \begin{bmatrix} i_d^\Delta & -i_q^\Delta & 4i_z^\Sigma & 0 & 4i_d^\Sigma \\ -i_q^\Delta & -i_d^\Delta & 0 & 4i_z^\Sigma & 4i_q^\Sigma \\ i_d^\Delta & i_q^\Delta & 2i_d^\Sigma & 2i_q^\Sigma & 4i_z^\Sigma \end{bmatrix}. \quad (23)$$

4) *Arm capacitor voltages difference*: Finally, the steady-state time invariant dynamics of the voltage difference vectors \mathbf{v}_{Cdq}^Δ and v_{CZ}^Δ are now recalled. Results are obtained by applying the Park transformation at ω and 3ω to (10). For the sake of compactness, the voltage difference vector is defined as $\mathbf{v}_{Cdqz}^\Delta \stackrel{\text{def}}{=} \left[v_{Cd}^\Delta, v_{Cq}^\Delta, v_{CZd}^\Delta, v_{CZq}^\Delta \right]^\top$.

$$C_{arm} \frac{d\mathbf{v}_{Cdqz}^\Delta}{dt} = i_{mdqz}^\Delta - \begin{bmatrix} \mathbf{J}_\omega & \mathbf{0}_{2 \times 2} \\ \mathbf{0}_{2 \times 2} & 3\mathbf{J}_\omega \end{bmatrix} C_{arm} \mathbf{v}_{Cdqz}^\Delta \quad (24)$$

with i_{mdqz}^Δ representing the modulated current as defined in (25), as a function of the modulation indexes,

$$i_{mdqz}^\Delta = \frac{1}{16} \mathbf{I}^\Delta \left[\mathbf{m}_{dq}^\Delta{}^\top, \mathbf{m}_{dq}^\Sigma{}^\top, m_z^\Sigma \right]^\top. \quad (25)$$

I^Δ is the following 4×5 time-invariant current matrix:

$$I^\Delta \stackrel{\text{def}}{=} \begin{bmatrix} 2i_d^\Sigma + 4i_z^\Sigma & -2i_q^\Sigma & i_d^\Delta & -i_q^\Delta & 2i_d^\Delta \\ -2i_q^\Sigma & -2i_d^\Sigma + 4i_z^\Sigma & -i_d^\Delta & -i_q^\Delta & 2i_q^\Delta \\ 2i_d^\Sigma & 2i_q^\Sigma & i_d^\Delta & i_q^\Delta & 0 \\ -2i_q^\Sigma & 2i_d^\Sigma & i_q^\Delta & -i_d^\Delta & 0 \end{bmatrix}. \quad (26)$$

5) *DC bus dynamics*: The DC bus dynamics are modelled by (27), where C_{dc} is the cable model terminal capacitance and P_l represents the power injection as seen from the MMC station.

$$C_{dc} \frac{dv_{dc}}{dt} = \frac{P_l}{v_{dc}} - 3i_z^\Sigma \quad (27)$$

An overview of the model structure corresponding to the MMC and DC bus equations is shown in Fig. 3.

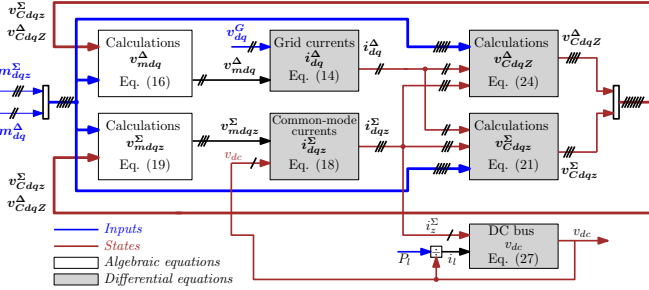


Figure 3. MMC and DC bus equations resume

III. MMC MODEL WITH CLASSICAL CCSC AND DC VOLTAGE DROOP

This section presents the control scheme for an MMC as shown in Fig. 4. For the AC-side, the MMC control strategy is based on a classical scheme with two cascaded loops. The outer loop controls the active power P_{ac} following a $P_{ac}-v_{dc}$ droop characteristic with gain k_d [14], and reactive power Q_{ac} .

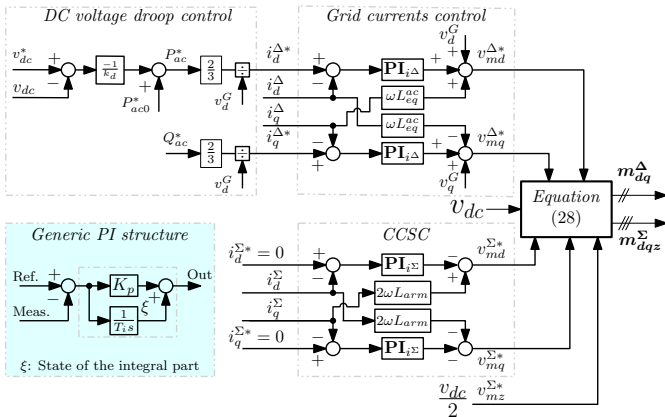


Figure 4. MMC droop-controlled with Classical CCSC

The inner loops control the AC currents in dq frame. The variables v_{md}^* and v_{mq}^* are the output of the controllers regulating the grid side current i_{dq}^Δ to the desired reference $i_{dq}^{\Delta*}$ by implementing standard current controllers with decoupling feed-forward terms. This controller is tuned to have a response time τ_i^Δ of 10 ms with a damping coefficient ζ_i^Δ of 0.7.

Furthermore, $v_{md}^{\Sigma*}$ and $v_{mq}^{\Sigma*}$ are the outputs of the CCSC [5], forcing the circulating currents i_{dq}^Σ to zero. The gains of the controllers are calculated to achieve a response time τ_i^Σ of 5 ms and ζ_i^Σ of 0.7. The output DC current of the converter is left uncontrolled with this strategy, and it is naturally adjusted to balance the AC and DC power flow.

The MMC insertion indexes are calculated directly from the output of the control loops for the ac-side and CCSC as shown in (28).

$$m_d^\Sigma = 2 \frac{v_{md}^{\Sigma*}}{v_{dc}}, \quad m_q^\Sigma = 2 \frac{v_{mq}^{\Sigma*}}{v_{dc}}, \quad m_z^\Sigma = 2 \frac{v_{mz}^{\Sigma*}}{v_{dc}} \quad (28a)$$

$$m_d^\Delta = -2 \frac{v_{md}^{\Delta*}}{v_{dc}}, \quad m_q^\Delta = -2 \frac{v_{mq}^{\Delta*}}{v_{dc}} \quad (28b)$$

where, for this controller, m_z^Σ is equal to 1 and v_{dc} is the measured DC voltage. Instead of v_{dc} , a fixed value (i.e. the nominal voltage) can be used, but this choice can reduce the stability region of the MMC [9]. Calculation of the insertion indexes in this way will be referred to as the ‘‘Un-Compensated Modulation’’ (UCM) [17], since there is no compensation for the impact of the oscillations in the equivalent arm capacitor voltages on the modulated output voltages.

IV. SMALL SIGNAL STABILITY ANALYSIS OF AN MMC WITH CLASSICAL CCSC

A. Model linearization and time domain validation

The non-linear time-invariant model presented in Section II with the control from Section III are connected as shown in Fig. 5.

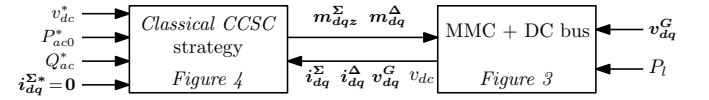


Figure 5. Non-linear time-invariant model of MMC, DC bus and Classical CCSC

This interconnected model is represented by a subset of ordinary differential equation f as expressed in (29), where x represents the states of the system as in (30) and u the inputs as in (31).

$$\dot{x}(t) = f(x(t), u(t)) \quad (29)$$

$$x = [\underbrace{\xi_{i_{dq}^\Delta} \xi_{i_{dq}^\Sigma}}_{\text{Controllers}} \underbrace{i_{dq}^\Delta i_{dqz}^\Sigma v_{cdqz}^\Sigma v_{cdqz}^\Delta}_{\text{MMC}} \underbrace{v_{dc}}_{\text{DC bus}}]^\top \quad (30)$$

$$u = [\underbrace{v_{dc}^* P_{ac}^* Q_{ac}^* i_d^{\Sigma*} i_q^{\Sigma*}}_{\text{Controllers}} \underbrace{v_d^G v_q^G}^\top_{\text{AC grid}}]^\top \quad (31)$$

The non-linear model from (29) can be linearized around a steady-state operating point by means of the Jacobian linearization method, resulting in a Linear Time-Invariant (LTI) representation as expressed in (32) [18]. It is recalled that each element A_{ij} and B_{ij} of the matrices A and B are related to the equations f as shown in (33).

$$\Delta \dot{x}(t) = A(x_0, u_0) \Delta x(t) + B(x_0, u_0) \Delta u(t) \quad (32)$$

$$A_{ij} = \left. \frac{\partial f_i(x, u)}{\partial x_j} \right|_{(x_0; u_0)}; \quad B_{ij} = \left. \frac{\partial f_i(x, u)}{\partial u_j} \right|_{(x_0; u_0)} \quad (33)$$

The equilibrium point, defined by (x_0, u_0) , is calculated from the direct resolution of the system equations from (29) by setting $\dot{x}(t)$ equal to zero. The obtained LTI model is used for evaluating small-signal dynamics and stability by eigenvalue analysis.

To validate the developed small-signal model of the MMC with *Classical CCSC*, results from a time-domain simulation of two different models will be shown and discussed in the following:

- 1) *EMT*: The system from Fig. 1 implemented in EMT-P-RV with 400 submodules. The MMC is modeled with the so-called “Model # 2: *Equivalent Circuit-Based Model*” from [15]. It is worth noticing that the modulation indexes are transformed from “ Σ - Δ ” and dq frame to “Upper-Lower” and abc frame.
- 2) *LTI*: This model represents the linearized time-invariant model of the interconnected system from Fig. 5, implemented in Matlab/Simulink. The operating point corresponds to the nominal ratings.

The main system parameters are listed in Table II.

Table II
PARAMETERS FOR THE TIME DOMAIN SIMULATION

U_{1n}	320 kV	R_f	0.521 Ω	$\tau_{i_d}^\Delta$	10 ms
P_n	1 GW	L_f	58.7 mH	$\zeta_{i_d}^\Delta$	0.7
f_n	50 Hz	R_{arm}	1.024 Ω	$\tau_{i_z}^\Sigma$	5 ms
C_{arm}	32.55 μ F	L_{arm}	48 mH	$\zeta_{i_z}^\Sigma$	0.7
C_{dc}	195.3 μ F	v_{dcn}	640 kV	k_d	0.1 pu

Starting with a DC power transfer of 1 pu (from DC to AC), a step is applied on P_l of -0.1 pu at 0.05 s. The reactive power is controlled to zero during the event. Simulation results are gathered in Fig. 6.

The dynamic response of the DC power P_{dc} is shown in Fig. 6(a) (i.e. measured power in the reference model and the calculated power for the linearized model as $P_{dc} = 3i_z^\Sigma v_{dc}$). The results of the common-mode currents are shown in Fig. 6(b) (only dq components). The EMT model presents oscillations at 6ω in steady state. These oscillations were neglected during the development of the time-invariant model [12]. As seen in the comparisons from Fig. 6(b), the model captures the average dynamics with reasonable accuracy even if the 6th harmonic components are ignored (notice the scale). For all other variables, there are negligible differences between the different models.

The step applied on P_l produces power imbalance in the DC bus, and the MMC reacts with the droop controller and its internal energy to achieve the new equilibrium point. The DC voltage results are shown in Fig. 6(c). Due to the DC voltage droop control (proportional controller with gain k_d), a steady-state error is obtained after the transient. The internal energy of the MMC participates in the dynamics of the DC voltage regulation by discharging its internal capacitors into the DC bus during the transients, as seen in the voltage $v_{C_z}^\Sigma$ from Fig. 6(d). The behavior of $v_{C_z}^\Sigma$ is similar to the DC bus voltage as expected from the discussion in [14].

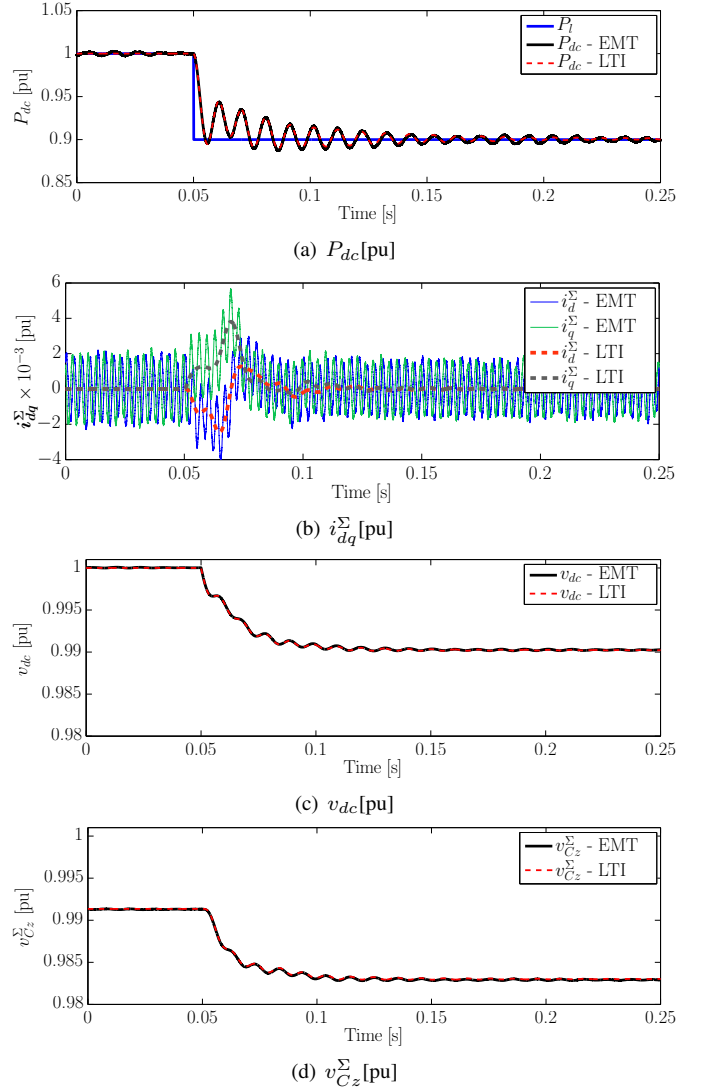


Figure 6. Time domain validation *Classical CCSC* – Step applied on P_l of 0.1 pu – *EMT*: EMT-P-RV simulation with detailed converter, *LTI*: Linear time-invariant state-space model in Simulink

B. Stability analysis

Since the linearized model from Fig. 5 has been validated, it can be used for small signal stability analysis. The impact of three main parameters influencing the DC voltage dynamics are evaluated: the DC capacitance, the droop gain k_d [14] and the response time of the current loops.

1) *Influence of the DC capacitance*: In MTDC systems, the value of the equivalent DC capacitance depends on the number of MMC stations connected to the grid as well as the cable lengths [14]. This value may vary because some converters could be disconnected or the grid topology reconfigured. For this reason, the MMC should be able to operate under different situations that can result from changes of the DC grid topology and parameters. For evaluating the impact of the DC side capacitance on the small-signal stability, a parametric sweep is performed. The electrostatic constant H_{dc} is defined as,

$$H_{dc} = \frac{1}{2} C_{dc} \frac{v_{dcn}^2}{P_n}. \quad (34)$$

The value of H_{dc} is varied from 40 ms down to 5 ms. This last value represents a small capacitance of the DC bus ($24, 4\mu F \ll (6 \times C_{arm})$), which could represent the DC capacitance of a short cable. The first results consider a power direction from DC to AC side of 1 GW (1 pu) of power transfer. Results are shown in Fig. 7(a). In this case, for the selected values the system remains stable.

It is known that the converters dynamics depend on the operating point [19]. The same parametric sweep as the previous example is performed with the opposite power transfer direction (i.e. from AC to DC side). The results are shown in Fig. 7(b), demonstrating that the system becomes unstable when the equivalent DC capacitor decreases.

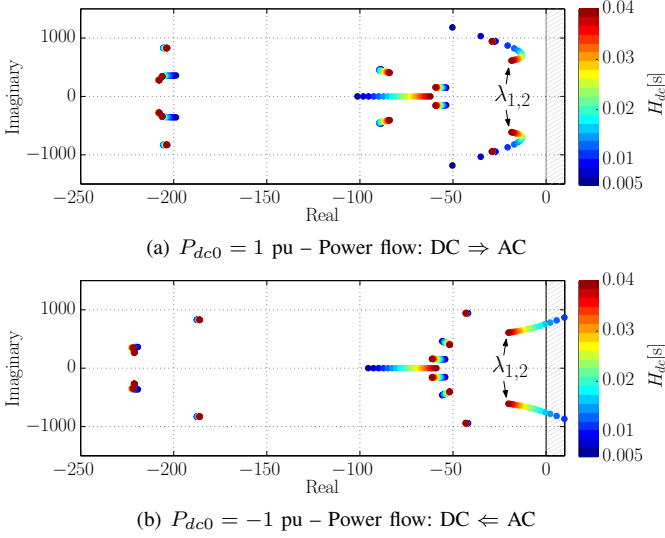


Figure 7. Parametric sweep of DC capacitor H_{dc} — DC Operating point $v_{dc0} = 1$ pu — $k_d = 0.1$ pu — Classical CCSC

2) *Influence of the droop parameter*: In this case, the droop parameter k_d is varied from 0.2 pu down to 0.05 pu. The considered power direction is from AC to DC since it is the worst case from the previous section. Results are shown in Fig. 8. When lower values of droop are used, the eigenvalues $\lambda_{1,2}$ shift to the right-hand plane (RHP) resulting in unstable behavior.

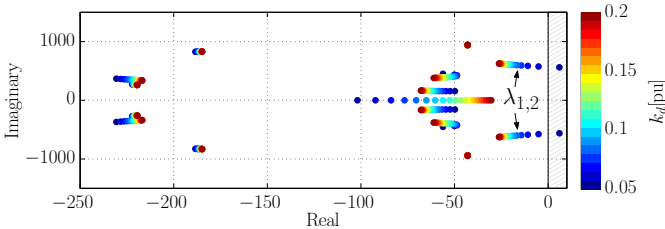


Figure 8. Parametric sweep of Droop parameter k_d — DC Operating point $v_{dc0} = 1$ pu, $P_{dc0} = -1$ pu — Classical CCSC

3) *Influence of current controllers*: For evaluating the impact of the current controllers on the stability, the response times of the grid current control loops (CCSC) are varied as well as the circulating current control loops (CCSC). Results are shown in Fig. 9(a) for the variation of τ_i^Δ and Fig. 9(b) for τ_i^Σ . When

faster controllers are used (lower values of response times), the eigenvalues $\lambda_{1,2}$ shift to the RHP.

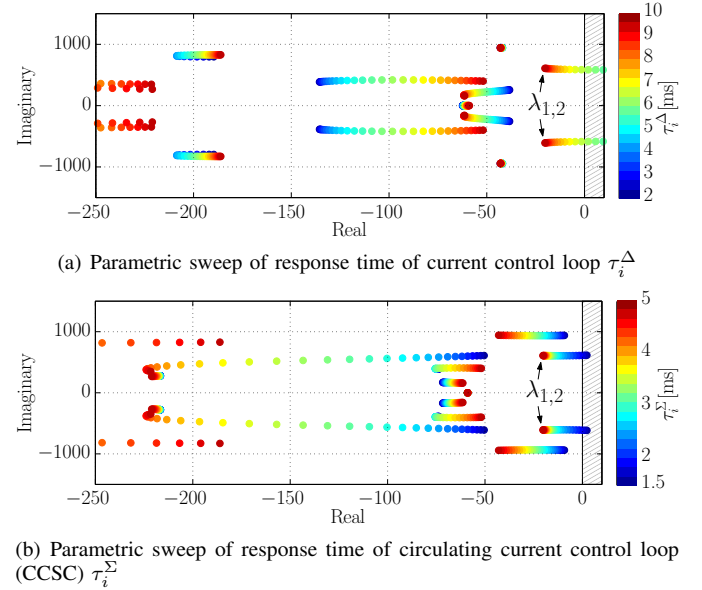


Figure 9. Parametric sweep of response time of current controllers — DC Operating point $v_{dc0} = 1$ pu, $P_{dc0} = -1$ pu

C. Identification of unstable eigenvalues

As observed in the previous results (Figs. 7, 8 and 9), the system may become unstable due to the same pair of eigenvalues for all cases ($\lambda_{1,2}$). For understanding the origin of these eigenvalues, participation factor analysis is performed for the case from the previous sub-section and the results are shown in Fig. 10, where the considered parameters and operating point are given in Table II.

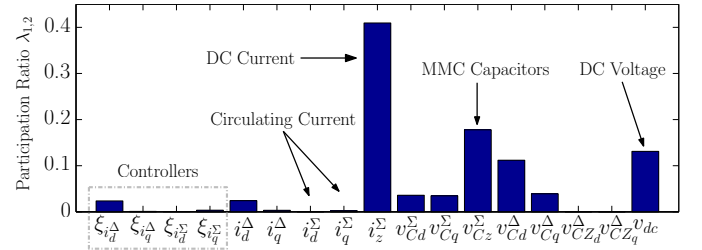


Figure 10. Results from participation factor analysis - Eigenvalues $\lambda_{1,2}$ — $\tau_i^\Delta = 10$ ms; $\tau_i^\Sigma = 5$ ms; $k_d = 0.1$ pu; $H_{dc} = 40$ ms

Results from Fig. 10 indicate that the states with the highest participation in the critical mode are i_z^Σ (i.e. the DC current), v_{Cz}^Σ (the state of the MMC which represents the internally stored energy) and v_{dc} (DC voltage). It shows also that the internal circulating currents i_{dq}^Σ do not have significant influence on these eigenvalues and neither do the integral part of the controllers (with the chosen bandwidths).

The impact of the proportional gains of the controllers are evaluated by calculating the participation factors for each point from Figs. 9 and the results are shown in Fig. 11. In Fig. 11(a), a similar pattern is observed for the participation factors as in Fig. 10. For fast response times of the CCSC, the dq

components of v_C^Σ participate more on the studied eigenvalues, but the system is unstable as shown in Fig. 9(b). Nevertheless, for realistic values of response times, the most important states are i_z^Σ , v_{Cz}^Σ and v_{dc} , which corresponds to the results in Fig. 10.

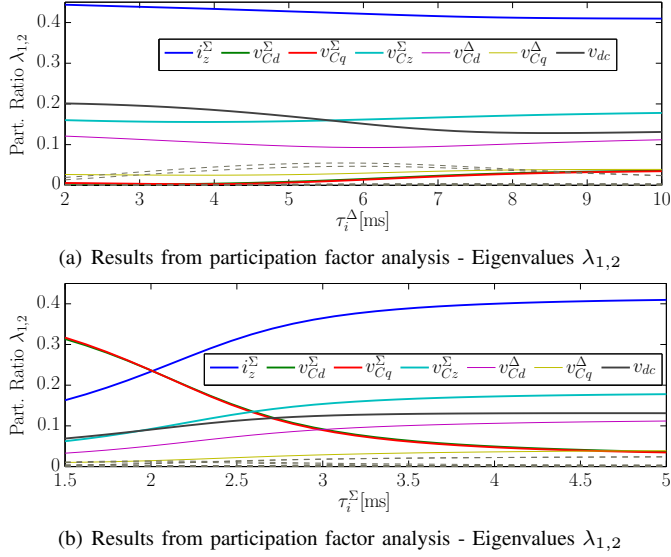


Figure 11. Participation factors for different response times — Dashed lines correspond to the states that are not listed in the legend — DC Operating point $v_{dc0} = 1$ pu, $P_{dc0} = -1$ pu

V. SMALL SIGNAL STABILITY IMPROVEMENT OF AN MMC WITH ENERGY BASED CONTROLLER

Since the instabilities identified in the studied cases are due mainly to the uncontrolled output current i_z^Σ , the natural further step is the explicit control of this current for improving the behavior of the system.

A. Energy-based controller

The considered control strategy from previous section control two out of three common-mode currents i^Σ . The uncontrolled zero-sequence component of i^Σ may cause interactions with the DC bus and the internal capacitor voltages, and can potentially make the system unstable. To improve the stability of the studied system, it is proposed to add a DC current control loop (or what is the same, a controller for i_z^Σ).

In the *Classical CCSC* strategy from last section, the energy is naturally following the DC bus voltage. The DC current is adjusting itself to achieve an implicit balance of energy and between AC and DC power in steady state. When controlling the DC current, this natural balance is lost so the DC current has to be determined explicitly to regulate the internally stored energy and balance the AC and DC power flow.

1) *Inner control loop — Z-sequence Σ current*: The design of the controller for i_z^Σ is based on the second equation of (18a), and a simple PI can be deduced as shown in Fig. 12. For tuning purposes, v_{mz}^Σ is supposed to be equal to $v_{mz}^{\Sigma*}$.

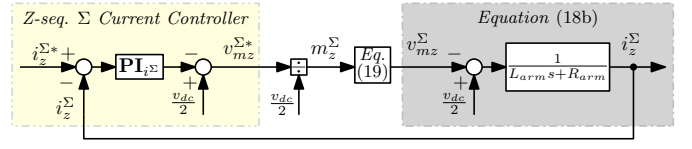


Figure 12. Block diagram of the i_z^Σ current control

2) *Outer control loop — Energy controller*: For generating the current reference $i_z^{\Sigma*}$ an outer loop is needed. The proposed strategy is based on the explicit control of the the total stored energy W_z^Σ on the MMC capacitors C_{arm} given by the power balance between AC and DC sides [16]. For designing this controller, a model with the explicit relation between the DC current i_{dc} and the total stored energy W_z^Σ is needed. Assuming $P_{ac}^* \approx P_{ac}$, a simplified expression of the sum energy dynamics can be defined as [16]:

$$\frac{dW_z^\Sigma}{dt} \approx P_{dc} - P_{ac} \approx v_{dc} \underbrace{3i_{dc}^\Sigma}_{i_{dc}} - P_{ac}^* \quad (35)$$

The deduced controller structure is shown in Fig. 14. For tuning purposes, the inner i_z^Σ current controller is considered as a unity gain.

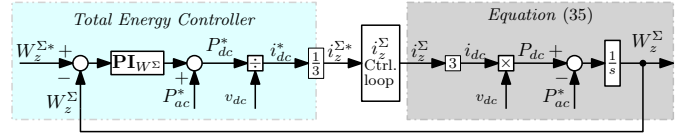


Figure 13. Controller design for W_z^Σ

Finally, the complete control structure is shown in Fig. 14, where the response time for the total energy τ_W^Σ is set to 50 ms (i.e. 10 times slower than the inner Σ current loop). The energy reference $W_z^{\Sigma*}$ is set to 1 pu in this paper, for maintaining a constant level of stored energy (corresponding to the rated capacitor voltages). As explained in [20], the energy W_z^Σ is

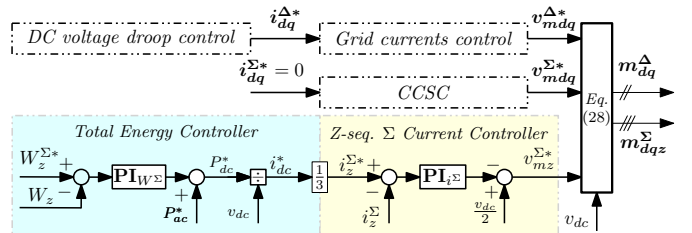


Figure 14. Complete *Energy based* control - Current and Energy controllers calculated from the dqz components as in (36).

$$W_z^\Sigma \approx C_{arm} \left(\frac{(v_{Cd}^\Sigma)^2}{2} + \frac{(v_{Cq}^\Sigma)^2}{2} + (v_{Cz}^\Sigma)^2 \right) + \dots \quad (36)$$

$$\dots + C_{arm} \sum_{k=d,q,Z_d,Z_q} \frac{(v_{Ck}^\Delta)^2}{2}$$

B. Model linearization and time domain validation

In a similar way as in Section IV, the system comprising the non-linear model from Fig. 3 and the controller from Fig. 14 are

connected as shown in Fig. 15. The state variables of the new controllers $\xi_{i_{\Sigma}^z}$ and $\xi_{W_{\Sigma}^z}$, which correspond to the integral part of the PI controllers, are concatenated to the system states \mathbf{x} . Also, the energy reference $W_z^{\Sigma*}$ is now included in the inputs vector \mathbf{u} . The new interconnected model can be linearized around any operating point for stability analysis.

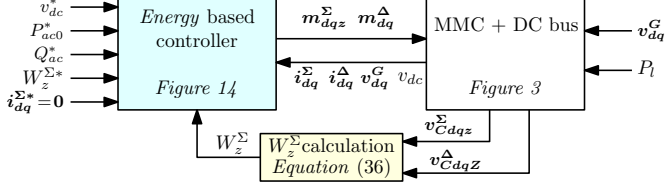


Figure 15. Non-linear time-invariant model of MMC, DC bus and *Energy based* controller

To validate the developed small-signal model of the MMC with *Energy based* control, results from time domain simulations are shown in Fig. 16. The event and parameters are the same as for Section IV, but it can be observed that the transient behavior of the DC power and voltage are well controlled contrary to the oscillatory behavior from the *Classical CCSC* strategy (Fig. 6).

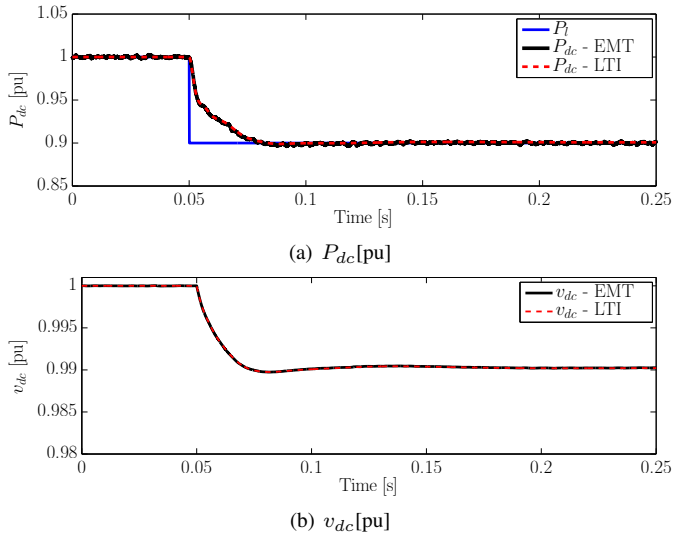


Figure 16. Time domain validation *Energy based* controller – Step applied on P_l of 0.1 pu – *EMT*: EMTP-RV simulation with detailed converter, *LTI*: Linear time-invariant state-space model in Simulink

C. Stability analysis with *Energy-based* controller

As shown in Section IV-B, when the *Classical CCSC* from Fig. 4 was considered, some instabilities were observed with low values of droop gain k_d or low equivalent capacitance on the DC side (i.e. low values of H_{dc}). For demonstrating the stability improvement with the *Energy-based* controller from Fig. 14, the same parametric sweep is performed as for Fig. 7 and Fig. 8. The results are gathered in Fig. 17. For both situations, it is only shown the case where the power flow is from the DC side to the AC side since it was the case where the instabilities occurred in Section IV-B. However, with

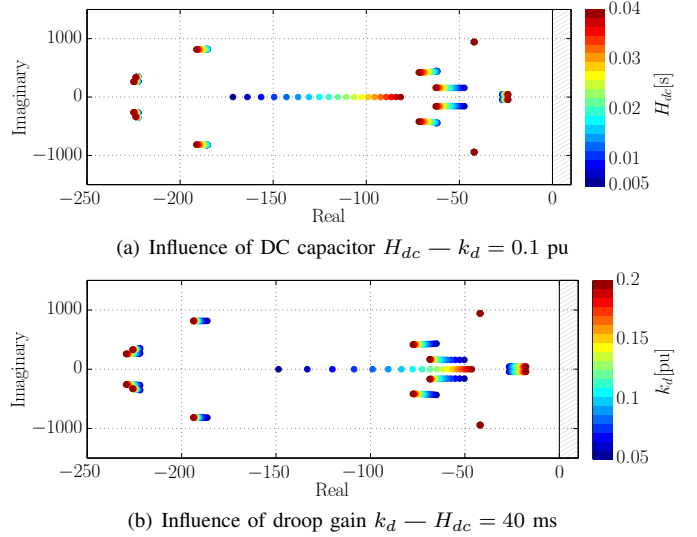


Figure 17. Parametric sweeps for *Energy-based control* — $v_{dc0} = 1$ pu, $P_{dc0} = -1$ pu, $k_d = 0.1$ pu — Power flow: DC \Leftarrow AC

this controller, the system presents similar behavior from both power directions.

For the case of the variation of H_{dc} in Fig. 17(a), as well for the variation of k_d in Fig. 17(b) it can be clearly observed that stability is guaranteed for the studied cases.

VI. STABILITY COMPARISON

A. DC Capacitance

For comparing the stability improvement, the eigenvalues from Fig. 7(b) and Fig. 17(a) with an electrostatic constant H_{dc} of 14.2 ms are shown in Fig. 18. The value of H_{dc} is chosen for highlighting the stability limits for the *Classical CCSC*. The unstable poles have a value of $2.81 \pm j781$, which corresponds to a frequency of 124 Hz approximately.

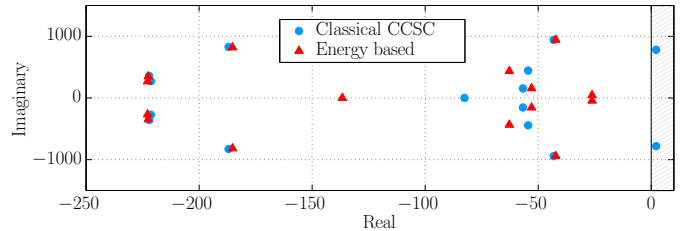


Figure 18. Eigenvalues comparison *Energy-based* and *Classical CCSC* control — DC Operating point $v_{dc0} = 1$ pu, $P_{dc0} = -1$ pu, Power flow: DC \Leftarrow AC — $k_d = 0.1$ pu

The stability improvements with the *Energy-based* controller are highlighted by a time domain simulation. The operating point is the same as for Fig. 18, and results are shown in Fig. 19. Since, for this set of parameters, the configuration of the MMC with *Classical CCSC* is unstable, the simulation is started with an extra capacitor connected in parallel with C_{dc} for stabilizing the system, which is disconnected at $t = 0$ s. The frequency of the oscillations corresponds to the frequency of the unstable eigenvalues from Fig. 18.

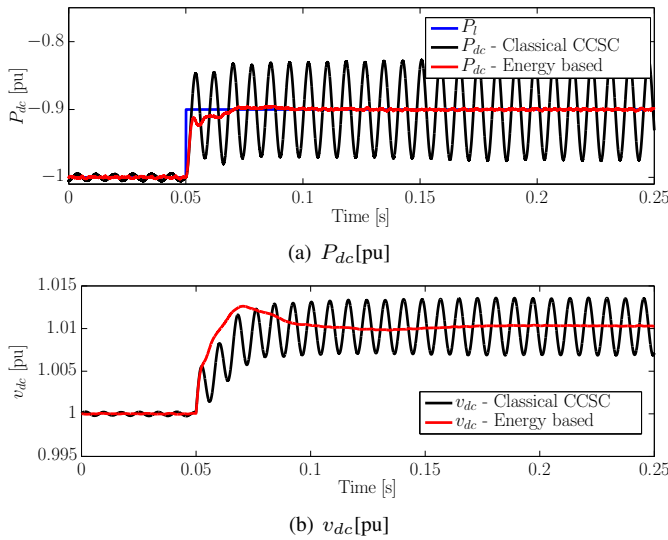


Figure 19. Time domain comparison in EMTF-RV with detailed converters with *Classical CCSC* and *Energy based* strategies — Step applied on P_l of 0.1 pu — $H_{dc} = 14.2$ ms

B. Active power reversal

In this section, an active power reversal from 1 pu to -1 pu is considered. Fixing a DC capacitance with H_{dc} equal to 10ms, and a droop parameter k_d equal to 0.1 pu, a parametric sweep for both control strategies is performed and the results are gathered in Fig. 20. For the *Classical CCSC* in Fig. 20(a) the system is unstable for DC power values lower than -0.15 pu approximately, whereas in Fig. 20(b), i.e. the case with *Energy based* controller, the system remains stable for all the power range.

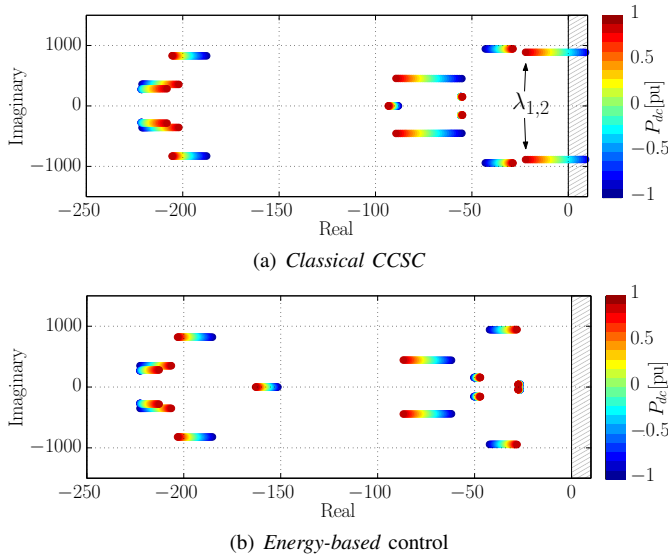


Figure 20. Parametric sweep of DC power reversal with *Classical CCSC* and *Energy based* strategies — $H_{dc} = 10$ ms — $k_d = 0.1$ pu

Results from Fig. 20 are validated in time domain simulations as shown in Fig. 21. The AC power reference P_{ac0}^* (see Fig. 4) is also ramped during the transient with the same rate for taking into account the voltage deviation. This represents the case where the power reversal signal is coordinated by a dedicated

MTDC master controller. The time domain results highlight the benefits of the *Energy based* control approach for improving the stability of the system.

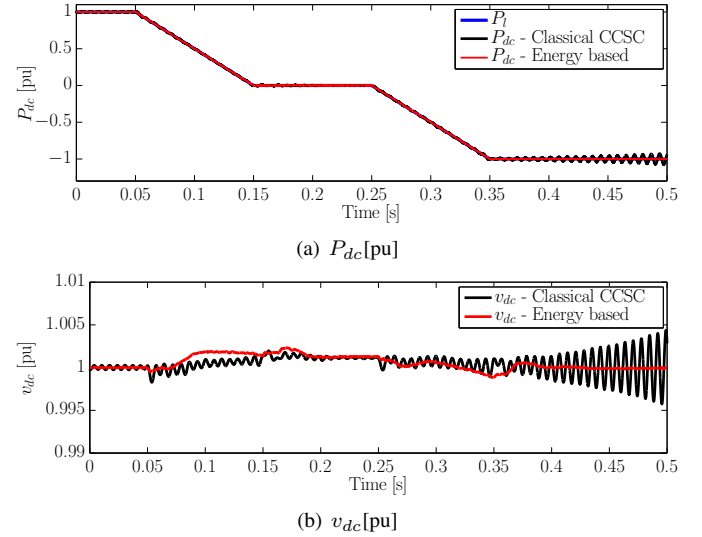


Figure 21. Time domain comparison in EMTF-RV with detailed converters with *Classical CCSC* and *Energy based* strategies — $H_{dc} = 10$ ms — $k_d = 0.1$ pu

VII. CONCLUSIONS

This paper has identified the source of the poorly damped and even possible unstable oscillations that can appear for MMCs relying on a CCSC without control of the internally stored energy. It has been demonstrated by participation factor analysis that the source of these potential stability problems is that the classical CCSC leaves the DC-side current uncontrolled, which leads to potential interaction with the DC bus voltage and the internally stored energy of the the MMC. To avoid these interactions, a control loop for regulating the energy stored in the MMC is introduced. The output of this control loop is the reference for controlling the DC-side current, which is corresponding to the zero-sequence component resulting from the dq- transformation used for the implementation of the classical CCSC. The stability improvement due to the additional control loops is clearly demonstrated by small-signal eigenvalue analysis based on linearization of the presented state-space model, which is accurately representing the internal dynamics of the MMC. The applied state-space modeling approach and the improved dynamic response obtained with the added energy- and DC-side current controllers is validated by time-domain simulations in comparison to a detailed EMT model of an MMC with 400 sub-modules per arm. Further developments should consider the dynamic analysis of a more advanced management of the energy in the MMC, i.e. where the energy sum and difference are explicitly controlled.

REFERENCES

- [1] A. Lesnicar and R. Marquardt, "An innovative modular multilevel converter topology suitable for a wide power range," in *Power Tech Conference Proceedings, 2003 IEEE Bologna*, vol. 3, pp. 6 pp. Vol.3–, June 2003.

- [2] A. Antonopoulos, L. Angquist, and H. P. Nee, "On dynamics and voltage control of the modular multilevel converter," in *Power Electronics and Applications, 2009. EPE '09. 13th European Conference on*, pp. 1–10, Sept 2009.
- [3] S. Debnath, J. Qin, B. Bahrani, M. Saeedifard, and P. Barbosa, "Operation, control, and applications of the modular multilevel converter: A review," *IEEE Transactions on Power Electronics*, vol. 30, pp. 37–53, Jan 2015.
- [4] K. Ilves, A. Antonopoulos, S. Norrga, and H.-P. Nee, "Steady-state analysis of interaction between harmonic components of arm and line quantities of modular multilevel converters," *IEEE Transactions on Power Electronics*, vol. 27, pp. 57–68, January 2012.
- [5] Q. Tu, Z. Xu, and J. Zhang, "Circulating current suppressing controller in modular multilevel converter," in *IECON 2010 - 36th Annual Conference on IEEE Industrial Electronics Society*, pp. 3198–3202, Nov 2010.
- [6] A. Jamshidifar and D. Jovcic, "Small signal dynamic dq model of modular multilevel converter for system studies," *Power Delivery, IEEE Transactions on*, vol. 31, pp. 191–199, February 2016.
- [7] T. Li, A. Gole, and C. Zhao, "Stability of a modular multilevel converter based hvdc system considering dc side connection," *IET Conference Proceedings*, pp. 21 (6)–21 (6) (1), January 2016.
- [8] N. R. Chaudhuri, R. Oliveira, and A. Yazdani, "Stability analysis of vector-controlled modular multilevel converters in linear time-periodic framework," *IEEE Transactions on Power Electronics*, vol. 31, pp. 5255–5269, July 2016.
- [9] J. Freytes, G. Bergna, J. Suul, S. D'Arco, H. Saad, and X. Guillaud, "Small-signal model analysis of droop-controlled modular multilevel converters with circulating current suppressing controller," in *13th IET International Conference on AC and DC Power Transmission (ACDC 2017)*, pp. 16–24, February 2017.
- [10] L. Harnefors, A. Antonopoulos, S. Norrga, L. Angquist, and H.-P. Nee, "Dynamic analysis of modular multilevel converters," *Industrial Electronics, IEEE Transactions on*, vol. 60, pp. 2526–2537, July 2013.
- [11] T. Li, A. M. Gole, and C. Zhao, "Harmonic instability in mmc-hvdc converters resulting from internal dynamics," *IEEE Transactions on Power Delivery*, vol. 31, no. 4, pp. 1738–1747, 2016.
- [12] G. Bergna, J. A. Suul, and S. D'Arco, "State-space modelling of modular multilevel converters for constant variables in steady-state," in *2016 IEEE 17th Workshop on Control and Modeling for Power Electronics (COMPEL)*, pp. 1–9, June 2016.
- [13] J. Beerten, S. D'Arco, and J. A. Suul, "Identification and small-signal analysis of interaction modes in vsc mtdc systems," *IEEE Transactions on Power Delivery*, vol. 31, pp. 888–897, April 2016.
- [14] J. Freytes, P. Rault, F. Colas, F. Gruson, and X. Guillaud, "Dynamic impact of mmc controllers on dc voltage droop controlled mtdc grids," in *18th European Conference on Power Electronics and Applications (EPE)*, 2016.
- [15] H. Saad, S. Denetiere, J. Mahseredjian, P. Delarue, X. Guillaud, J. Peralta, and S. Nguéfeu, "Modular multilevel converter models for electromagnetic transients," *Power Delivery, IEEE Transactions on*, vol. 29, pp. 1481–1489, June 2014.
- [16] H. Saad, X. Guillaud, J. Mahseredjian, S. Denetiere, and S. Nguéfeu, "Mmc capacitor voltage decoupling and balancing controls," *IEEE Transactions on Power Delivery*, vol. 30, pp. 704–712, April 2015.
- [17] G. Bergna Diaz, J. A. Suul, and S. D'Arco, "Small-signal state-space modeling of modular multilevel converters for system stability analysis," in *Energy Conversion Congress and Exposition (ECCE), 2015 IEEE*, pp. 5822–5829, Sept 2015.
- [18] X.-F. Wang, Y. Song, and M. Irving, *Modern power systems analysis*. Springer Science & Business Media, 2010.
- [19] J. Freytes, S. Akkari, J. Dai, F. Gruson, P. Rault, and X. Guillaud, "Small-signal state-space modeling of an hvdc link with modular multilevel converters," in *2016 IEEE 17th Workshop on Control and Modeling for Power Electronics (COMPEL)*, pp. 1–8, June 2016.
- [20] J. Freytes, G. Bergna, J. A. Suul, S. D'Arco, H. Saad, and X. Guillaud, "State-space modelling with steady-state time invariant representation of energy based controllers for modular multilevel converters," in *IEEE PES PowerTech 2017, Manchester UK*, June 2017.

Julian Freytes (S'15) received the Electrical Engineering degree from the Universidad Nacional del Sur (UNS), Bahía Blanca, Argentina in 2013. He received the M.Sc. degree in Electrical Engineering for Sustainable Development from Université des Sciences et Technologies de Lille, France in 2014. Since 2015, he is pursuing his Ph.D on interoperability analysis of

Modular Multilevel Converters connected to Multi-Terminal DC grids in Ecole Centrale de Lille, France. His main research interests include the modeling and control of power electronics for HVDC systems.

Gilbert Bergna received his electrical power engineering degree from the "Simón Bolívar University", in Caracas, Venezuela, in 2008; his "Research Master" from SUPÉLEC (École Supérieure d'Électricité), in Paris, France, in 2010; and a joint PhD degree between SUPÉLEC and the Norwegian University of Science and Technology (NTNU) in 2015. In march 2014 he joined SINTEF Energy Research as a research scientist, and since august 2016 started a post-doctoral fellowship at NTNU working on control and modelling of power electronic systems.

Jon Are Suul (M'11) received the M.Sc. degree in Energy and Environmental Engineering and the PhD degree in Electric Power Engineering from the Norwegian University of Science and Technology (NTNU), Trondheim, Norway, in 2006 and 2012, respectively. From 2006 to 2007, he was with SINTEF Energy Research, until starting his PhD studies. From 2012 he resumed a position as a Research Scientist at SINTEF Energy Research, first in part-time while also working as a postdoctoral researcher at the Department of Electric Power Engineering of NTNU until 2016. His research interests are mainly related to modelling, analysis and control of power electronic converters in power systems and for renewable energy applications.

Salvatore D'Arco received the M.Sc. and Ph.D. degrees in electrical engineering from the University of Naples "Federico II", Naples, Italy, in 2002 and 2005, respectively. From 2006 to 2007, he was a postdoctoral researcher at the University of South Carolina, Columbia, SC, USA. In 2008, he joined ASML, Veldhoven, the Netherlands, as a Power Electronics Designer, where he worked until 2010. From 2010 to 2012, he was a postdoctoral researcher in the Department of Electric Power Engineering at the Norwegian University of Science and Technology (NTNU), Trondheim, Norway. In 2012, he joined SINTEF Energy Research where he currently works as a Research Scientist. His main research activities are related to control and analysis of power-electronic conversion systems for power system applications, including real-time simulation and rapid prototyping of converter control systems.

François Gruson received the Ph.D. degree in electrical engineering from the Ecole Centrale de Lille, Lille, in 2010. Since 2011, he has been working as Associate Professor at Arts and Metiers ParisTech in the Laboratoire d'Electrotechnique et d'Electronique de Puissance de Lille (L2EP), Lille, France. His research interests include power electronic converter and power quality for distribution and transmission grid application and especially for HVDC transmission grid.

Frédéric Colas was born in Lille, France, on October 17, 1980. He received his Ph.D. degree in control systems from Ecole Centrale de Lille, Lille, in 2007. He is a member of the Laboratory of Electrical Engineering (L2EP), Lille, and a Research Engineer at Arts et Metiers ParisTech. His research interests include the integration of dispersed generation systems in electrical grids, advanced control techniques for power systems, and hardware-in-the-loop simulation.

Hani Saad (S'07) received his B.Sc. and Ph.D. degrees in electrical engineering from the École Polytechnique de Montréal in 2007 and 2015, respectively. From 2008 to 2010 he worked at Techimp Spa. and in the Laboratory of Materials Engineering and High Voltages (LIMAT) of the University of Bologna on research and development activities. In 2014, he joined the French TSO RTE (Réseau de Transport d'Electricité), where he is currently involved in HVDC projects and EMT studies.

Xavier Guillaud (M'04) has been professor in L2EP - Lille since 2002. First, he worked on the modeling and control of power electronic systems. Then, he studied the integration of distributed generation and especially renewable energy in power systems. Nowadays, he is studying the high voltage power electronic converters in transmission system. He is leading the development of an experimental facility composed of actual power electronic converters interacting with virtual grids modelled in real-time simulator. He is involved on several projects about power electronic on the grid within European projects and different projects with French companies. He is member of the Technical Program Committee of Power System Computation Conference (PSCC) and associated editor of Sustainable Energy, Grids and Networks (SEGAN).